Barycentric spectral domain decomposition methods for valuing a class of infinite activity Lévy models

Edson Pindza[*], Francis Youbi[†], Eben Maré[‡], Matt Davison[§]

[*] [§]Department of Statistical and Actuarial Sciences, University of Western Ontario, London, Ont., Canada

[*] [§]Department of Applied Mathematics, University of Western Ontario, London, Ont., Canada

[†] [‡]Department of Mathematics and Applied Mathematics, University of Pretoria Pretoria 002, Republic of South Africa

Abstract

A new barycentric spectral domain decomposition methods algorithm for solving partial integro-differential models is described. The method is applied to European and butterfly call option pricing problems under a class of infinite activity Lévy models . It is based on the barycentric spectral domain decomposition methods, that allows the implementation of the boundary conditions in an efficient way. After the approximation of the spatial derivatives, we obtained the semi-discrete equations. The computation of these equations is performed by using the barycentric spectral domain decomposition method. This is achieved with the implementation of an exponential time integration scheme. Several numerical tests for the pricing of European and butterfly options are given to illustrate the efficiency and accuracy of this new algorithm. We also show that the option Greeks such as the Delta and Gamma sensitivity measures are computed with no spurious oscillation.

2010 Mathematics Subject Classification: 76M22, 41A10, 41A20, 91G80.

Keywords: Spectral methods, Clenshaw–Curtis quadrature, shifted Laguerre–Gauss quadrature, Domain decomposition, Partial integro-differential equation, Infinite activity Lévy processes.

1 Introduction

Option pricing problems are often modelled by stochastic processes. The famous stochastic model for the equilibrium condition between the expected return on the option, the expected return on the stock and the risk-free interest rate is the celebrated Black-Scholes equation derived by Black and Scholes in 1973 [5]. However, it is well known that constant volatility Black-Scholes model is not consistent with market prices. Therefore, more general models for stochastic dynamics of the risky assets have been developed. Among them we can mention, stochastic volatility models [19, 21], models with deterministic local volatility functions [8, 14] and Lévy models [25, 29, 27, 15, 34], including infinite activity Lévy models [15, 34]. Note that infinite activity Lévy models incorporate jumps whose intensity is not a finite measure.

Option problems under jump and Lévy models [25, 27] models can be modelled by means of Partial-integro Differential Equations (PIDEs). Due to inherent complexity in the modelling equations, one can rarely find closed-form analytical solutions to these models, and therefore one must resort to numerical methods. Briani *et al.* [6] used the fully explicit schemes, although their approach required very restrictive conditions for stability. Cont and Volchkova [10] used

[†]Corresponding author. E-mail: pindzaedson@yahoo.fr

implicit schemes to treat the differential part. The use of the Crank-Nicolson time stepping for the Partial Differential Equation (PDE) portion and explicit evaluation of the convolution integral term were tested by Tavella and Randall [38]. However, such an asymmetric treatment of PDE and integral part introduces biases in the viscosity solution such that second order convergence is not always achieved. d'Halluin *et al.* [12] employed the Crank-Nicolson scheme with Rannacher time smoothing to solve the PIDE. They used a fixed point iterative procedure as the system solver and obtained second order convergence. Tangman *et al.* [37] proposed an improved fourth order spectral discontinuity inclusion method. To get around the non-smooth initial condition, they clustered Chebyshev grid points at the discontinuous point and at boundaries. Pindza *et al.* [33], suggested that to overcome the problem of discontinuity and differentiability in the payoff at strike prices, the use of a grid refinement is one of the best tool to retain a satisfactory accuracy of the spectral method to numerically solve option pricing problems. Ngounda *et al.* employed the numerical inverse Laplace transform using the Bromwich contour integral approach to provide fast and accurate results for pricing European options with jumps.

In recent years, pure jump Lévy processes of infinite activity that governs stock market returns has been empirically and theoretically studied. These models are flexible enough to perfectly fit the market financial data and to capture the excess kurtosis and skewness arising from the risk-neutral distribution returns. The work done in [7] generalizes the VG model to the Carr, German, Madan and Yor (CGMY) model. The model has a jump component which follows a dynamics that can represent either finite or infinite activity of either finite or infinite variation. They also demonstrated that a diffusion component is not needed if the infinity activity jump process has finite variation. In the literature, finite difference schemes are mostly used for solving infinite activity Lévy PIDE problems. Wang *et al.* [43] proposed implicit FD methods for the numerical solution of the CGMY model. Almendral *et al.* [1] used FD methods to discretise the equation in space by the collocation method and using explicit difference backward schemes focused on the case of infinite activity and finite variation. Very recently, Fakharany *et al.* [15] developed an efficient finite difference scheme for partial integro-differential models related to European and American option pricing problems under a wide class of infinity Lévy models.

This paper proposes a study of a new barycentric spectral domain decomposition methods algorithm for solving partial integro-differential equations (PIDE) related to European and butterfly option pricing problems under a class of infinite activity Lévy models. The method is based on barycentric spectral domain decomposition methods, which allow the implementation of the boundary conditions in an efficient way. The system semi-discretised of ordinary differential equations, obtained after approximation of the spatial derivatives using barycentric spectral domain decomposition methods are solved, using an exponential time integration (ETI) scheme. Furthermore, the paper provides several numerical tests which show the superiority of this method over the popular Crank–Nicolson method. Various numerical results for the pricing of European and butterfly options are also given to illustrate the efficiency and accuracy of this new algorithm. We show that the option Greeks such as the Delta and Gamma sensitivity measures are efficiently computed to high accuracy.

The paper unfolds as follows. In Section 1, we provide a review of Lévy processes in finance and various numerical approaches to pricing options on assets these processes. In Section 2, we present some mathematical details of the fundamental approach we use to price European options on infinite activity Lévy processes. In Section 3, we provide a quick review of domain decomposition methods (other techniques such as barycentric spectral methods and finite difference methods are reviewed in Appendix A). In Section 4, we show how the continuous PIDE of Section 2 must be discretised using the domain decomposition methods of Section 3 resulting in a system of ordinary differential equations. Next, we discuss the use of exponential time differencing schemes to solve

the resulting system of ordinary differential equations. Section 5 provides numerical results to some representative problems which illustrate the advantages of the new methods as compared to more standard finite difference methods. The conclusions are provided in Section 6.

2 The jump-diffusion model

We assume an arbitrage-free market model with a single risky asset with price process $\{S_t\}_{t\in[0,T]}$ following an exponential Lévy model of the form

$$S_t = S_0 e^{X_t}, \tag{2.1}$$

on the filtered probability space $(\Omega, \mathcal{F}, \{\mathcal{F}_t\}_{t\in[0,T]}, \mathbb{P})$ where the Lévy process $\{X_t\}_{t\in[0,T]}$ has dynamics given by

$$X_t = \left(\mu - \frac{\sigma^2}{2} - \delta\right) t + \sigma W_t + \sum_{k=1}^{N_t} Y_k. \tag{2.2}$$

The jump process is represented by $J_t = \sum_{k=1}^{N_t} Y_k$ with $\{N_t\}_{t\in[0,T]}$ denoting a Poisson process with intensity $\lambda > 0$ and $\{Y_k\}_{k\geq 1}$ which are independent observations from a jump size variable Y.

Let consider $V(S,t)$ be the option value with the underlying asset S_t and T be the time to maturity. Under the equivalent risk neutral measure $\mathbb{Q} \sim \mathbb{P}$, the asset price $\{S_t\}_t \in [0,T]$ has the form (2.1), where X_t is now given by Equation (2.2), the value for a European option with strike price K is its discounted expected payoff

$$V(S,t) = e^{-r(T-t)} \mathbf{E}^{\mathbb{Q}} \left[\Psi(S_T)|S_t = S\right], \tag{2.3}$$

where $\Psi(S_T)$ is the payoff function. The value of a contingent claim $V(S,t)$ on the underlying asset S then solves the PIDE given by

$$V_t + \mathcal{L}V(S,t) = 0, \quad (S,t) \in \mathbb{R}_+ \times (0,T], \tag{2.4}$$

where the operator $\mathcal{L}$ is defined as

$$\mathcal{L}V(S,t) = \frac{\sigma^2}{2} S^2 V_{SS} + (r-q) S V_S - rV + \int_{-\infty}^{+\infty} f(y)[V(Se^y,t) - V(S,t) - S(e^y - 1)V_S(S,t)]dy. \tag{2.5}$$

The function $f(y)$ is the Lévy density function given in Table 1. The boundary and the initial conditions encode the difference between American and European style options as well as between puts and calls, and other types of options.

For European vanilla call options, the initial and the boundary conditions are given by

$$V(S,0) = \max(S-K,0), \quad V(0,t) = 0, \quad V(S,t) = S\mathrm{e}^{-qt} - K\mathrm{e}^{-rt}, \quad \text{as} \quad S \to \infty. \tag{2.6}$$

where K is the strike price.

A butterfly spread is a neutral strategy that has a combination of a bull spread and a bear spread. It is a limited profit, limited risk options strategy. There are three strike prices (discontinuities) involved in a butterfly spread and it can be constructed using calls or puts. The initial and boundary conditions of butterfly spread options are expressed as

$$V(S,0) = \max(S-K_1,0) - 2\max(S-K_2,0) + \max(S-K_3,0), \quad V(0,t) = 0, \quad V(S,t) = 0, \tag{2.7}$$

Model	Lévy density function
KoBol	$f(y) = \frac{C_- e^{-G\|y\|}}{\|y\|^{1+Y}} \mathbf{1}_{y<0} + \frac{C_+ e^{-M\|y\|}}{\|y\|^{1+Y}} \mathbf{1}_{y>0}$
Meixner	$f(y) = \frac{Ae^{-ay}}{y \sinh(by)}$
GH process	$f(y) = \frac{e^{\beta y}}{\|y\|} \left(\int_0^\infty \frac{e^{-\sqrt{2\zeta+\alpha^2}\|y\|}}{\pi^2 \zeta \left(J^2_{\|\lambda\|}(\delta\sqrt{2\zeta}) + Y^2_{\|\lambda\|}(\delta\sqrt{2\zeta}) \right)} d\zeta + \max(0,\lambda) e^{-\alpha\|y\|} \right)$

Table 1: Density functions for Lévy Processes

where S is the stock price K_1, K_2 and K_3 are three distinct strike prices such that $0 < K_1 < K_2 < K_3$, with $K_2 = (K_1 + K_3)/2$. In the *KoBoL model* [7], singularities are observed in the kernel of integration. This model is known as the Carr, German, Madan and Yor (CGMY) [7] when the parameters are set to be $C_- = C_+ = C > 0$, $G > 0, M > 0$ and $Y \in [0, 2)$. The parameter C indicates the overall level of activity. The parameters G and M are the measures depicting the skewness of the Lévy density such that $G = M$ yields a symmetric distribution. When choosing $G \neq M$ this leads to skewed distributions. The parameter Y describes the fine structure of the stochastic process. At $Y = -1$, the *KoBoL model* leads to a special case of Kou's double exponential model [15]. Furthermore, for $Y = 0$, we obtain the variance Gamma process. In a case of $Y \in (0, 1)$, infinite activity models with finite variation are obtained and in a case of $Y \in [1, 2]$, infinite activity models with infinite variation are depicted. There exist other singular kernel of integration Lévy processes. Meanwhile, the *hyperbolic and generalized hyperbolic* (GH) are used to obtain better estimation for the stock returns [47]. Here, the functions $J_\nu(\cdot)$ and $Y_\nu(\cdot)$ are the Bessel functions of first and second kind, respectively. The *Meixner* process was introduced in 1998 to model cases in which the environment is changing stochastically over time. The *Meixner* process was shown to be a reliable valuation for some indices such as Nikkei 225 [45, 46].

3 Domain decomposition

Challenges arise when we want to approximate a function with a jump discontinuity by using a high order finite difference methods or spectral methods. In general, the jump locations of a function and its derivatives are not explicitly known and computationally expensive methods have to be used to detect the location of these jumps [18]. Meanwhile, the case of infinite activity Lévy models option pricing problems, these discontinuities are located at strike prices and singularities of the density functions. Therefore, spectral domain decomposition methods [28] can be used to recover the accuracy at discontinuity points. Following [32, 28], the domain $\mathcal{D} = [a, b]$ can be broken into M sub-domains

$$\mathcal{D}_1 = (x^{(0)}, x^{(1)}), \mathcal{D}_2 = (x^{(1)}, x^{(2)}), ..., \mathcal{D}_M = (x^{(M-1)}, x^{(M)}),$$

with $x^{(0)} = a, x^{(M)} = b$. In general, $\mathcal{D}$ is covered by M sub-domains as

$$\mathcal{D} = \bigcup_{\mu=1}^{M} \mathcal{D}_\mu, \tag{3.8}$$

where each sub-domains has its own set of basis functions and expansion coefficients

$$u^{(\mu)}(x) = \sum_{k=0}^{N_\mu} \tilde{u}_k^{(\mu)} \phi_k^{(\mu)}(x), \quad x \in \mathcal{D}_\mu, \quad \mu = 1, ...M. \tag{3.9}$$

The notation $u^{(\mu)}$ represents the approximation in the μth domain, and the different sub-domains $\mathcal{D}_\mu$ can touch or overlap each other. For example, to solve a second order non-linear elliptic PDE or system of equations

$$(\mathcal{N}u)(x) = 0, \quad x \in \mathcal{D}, \tag{3.10}$$

in some domain $\mathcal{D} \subset \mathbb{R}^d$ with boundary conditions

$$g(u)(x) = 0 \quad x \in \partial\mathcal{D},$$

where $\mathcal{N}$ and d respectively denote the elliptic operator and mappings, the matching conditions must be satisfied. Hence, each function $u^{(\mu)}$, defined only on the single sub-domain $\mathcal{D}_\mu$, must fit together to form a smooth solution of (3.10) over the full domain $\mathcal{D}$. For infinite resolution, the following conditions at the limit must hold [32]:

1. When two sub-domains, $\mathcal{D}_\mu$ and $\mathcal{D}_\nu$, touch each other (patching), on their intersection surface the function and its derivative must be smooth, hence

$$\left\{ \begin{array}{rcl} u^\mu(x) & = & u^\nu(x) \\ \frac{\partial u^\mu}{\partial n}(x) & = & -\frac{\partial u^\nu}{\partial n}(x) \\ x & \in & \partial\mathcal{D}_\mu \cap \partial\mathcal{D}_\nu. \end{array} \right. \tag{3.11}$$

2. When two sub-domains, $\mathcal{D}_\mu$ and $\mathcal{D}_\nu$, overlap each other (overlapping), the functions $u^{(\mu)}$ and $u^{(\nu)}$ must be identical in $\mathcal{D}_\mu \cap \mathcal{D}_\nu$. Since the solution of a PDE is unique, we must prove that, at a boundary of the overlapping domain,

$$u^{(\mu)}(x) = u^{(\nu)}(x) \quad x \in \partial(\mathcal{D}_\mu \cap \mathcal{D}_\nu). \tag{3.12}$$

In this paper, we restrict ourself to the patching methods. The calculation of the integral part can be estimated over multi-domains as follows

$$\begin{aligned} \int_{\mathcal{D}} u(x)dx &= \int_{\bigcup_{\mu=1}^M \mathcal{D}_\mu} u^{(\nu)}(x)dx = \sum_{\nu=1}^M \int_{\mathcal{D}_\nu} u^{(\nu)}(x)dx \\ &\approx \sum_{\nu=1}^M \int_{\mathcal{D}_\nu} p_N^{(\nu)}(x)dx = \sum_{\nu=1}^M \int_{\mathcal{D}_\nu} \frac{\sum_{j=0}^N \frac{\omega_j^{(\nu)}}{x-x_j} u_j^{(\nu)}}{\sum_{j=0}^N \frac{\omega_j^{(nu)}}{x-x_j}} dx = \sum_{\nu=1}^M \sum_{j=0}^N \lambda_j^{(\nu)} u_j^{(\nu)}. \end{aligned} \tag{3.13}$$

In the next section we discretise the PIDE (2.4) by means of spectral domain decomposition methods.

4 Discretisation of the PIDE

Let us begin this section by transforming the PIDE (2.4) into a simpler one. Since the kernel of the integral in (2.4) presents a singularity at $y = 0$, a useful technique is to split the real line, for an arbitrary small parameter $\varepsilon > 0$, into two regions $\Omega_1 = [-\varepsilon, \varepsilon]$ and $\Omega_2 = \mathbb{R}\backslash\Omega_1$ (the complementary set of Ω_1 in the real line). The integral on Ω_1 is replaced by a suitable coefficient in the diffusion term of the differential part of (2.4) obtained by Taylor expansion of $V(Se^y, \tau)$ about S, see [11, 9]. This coefficient depending on ε is a convergent integral and takes the form

$$\breve{\sigma}^2(\varepsilon) = \int_{-\varepsilon}^{\varepsilon} f(y)(e^y - 1)^2 dy = \varepsilon \int_{-1}^{1} f(\varepsilon\phi)(e^{\varepsilon\phi} - 1)^2 d\phi, \quad -1 \leqslant \varepsilon \leqslant 1. \tag{4.1}$$

Letting $\tau = T - t$, the resulting approximating PIDE from (2.4) is given by

$$\frac{\partial C}{\partial \tau} = \frac{\hat{\sigma}^2}{2} S^2 \frac{\partial^2 C}{\partial S^2} + (r - q - \gamma(\varepsilon)) S \frac{\partial C}{\partial S} - (r + \chi(\varepsilon)) C + \int_{\Omega_2} f(y) C(Se^y, \tau) dy, \tag{4.2}$$

where

$$\hat{\sigma}^2 = \sigma^2 + \breve{\sigma}^2(\varepsilon), \quad \gamma(\varepsilon) = \int_{\Omega_2} f(y)(e^y - 1) dy, \quad \chi(\varepsilon) = \int_{\Omega_2} f(y) dy. \tag{4.3}$$

The approximation of $\breve{\sigma}^2$ in (4.1) is evaluated using the Clenshaw-Curtis quadrature and it is given by

$$\breve{\sigma}^2(\varepsilon) \approx \varepsilon \sum_{k=1}^{N} \lambda_k f(\varepsilon \phi_k)(e^{\varepsilon \phi_k} - 1)^2, \tag{4.4}$$

where $\phi_k = \cos\left(\frac{k\pi}{N}\right)$, and λ_k, $k = 0, 1, 2, ..., N$, are the Chebyshev-Gauss-Lobatto (CGL) nodes and the Clenshaw-Curtis weights [17, 41], respectively. The improper integrals $\chi(\varepsilon)$ and $\gamma(\varepsilon)$ in (4.3) are approximated using the shifted Laguerre–Gauss quadrature [16]. Under consideration of the change of variables $\eta = -y - \varepsilon$ for $y < 0$ and $\eta = y - \varepsilon$ for $y > 0$, the expressions $\chi(\varepsilon)$ and $\gamma(\varepsilon)$ have the following forms

$$\chi(\varepsilon) = \int_0^{\infty} (f(-\eta - \varepsilon) + f(\eta + \varepsilon)) d\eta \approx \sum_{k=1}^{N} \bar{\lambda}_k F(\eta_k, \varepsilon), \tag{4.5}$$

and

$$\gamma(\varepsilon) = \int_0^{\infty} [f(-\eta - \varepsilon)(e^{-(\eta+\varepsilon)} - 1) + f(\eta + \varepsilon)(e^{\eta+\varepsilon} - 1)] d\eta \approx \sum_{k=1}^{N} \bar{\lambda}_k G(\eta_k, \varepsilon), \tag{4.6}$$

where

$$F(\eta, \varepsilon) = e^{\eta}(f(-\eta - \varepsilon) + f(\eta + \varepsilon)),$$
$$G(\eta, \varepsilon) = e^{\eta}\left(f(-\eta - \varepsilon)(e^{-(\eta+\varepsilon)} - 1) + f(\eta + \varepsilon)(e^{\eta+\varepsilon} - 1)\right).$$

Here η_k are the roots of the Laguerre polynomial $L_N(\eta)$ of degree N defined by

$$L_N(\eta) = \frac{e^{\eta}}{N!} \frac{d^N}{\eta^N}\left(\eta^N e^{-\eta}\right), \tag{4.7}$$

and the weights $\bar{\lambda}_k, k = 1, 2, \ldots N$, are determined as in [16] by

$$\bar{\lambda}_k = \frac{1}{\eta_k \left(L'_N(\eta_k)\right)^2} = \frac{\eta_k}{(N+1)^2 \left(L_{N+1}(\eta_k)\right)^2}. \tag{4.8}$$

4.1 Discretisation of the PIDE on a single domain

We transform the PIDE (4.2) into a constant coefficient PIDE using the transformation $S = Ke^x$ and $u(x, \tau) = V(S, t)$. One obtains

$$u_\tau - \mathcal{L}u(x, \tau) = 0, \quad (x, \tau) \in \mathbb{R} \times (0, T] \tag{4.9}$$

where

$$\mathcal{L}u(x, \tau) = \frac{1}{2}\hat{\sigma}^2 u_{xx} + \left(r - q - \frac{1}{2}\hat{\sigma}^2 - \gamma(\varepsilon)\right) u_x - (r + \chi(\varepsilon)) u + \int_{\Omega_2} u(x + y, \tau) f(y) dy \tag{4.10}$$

We define the numerical domain by $\mathcal{D} = [y_M, y_m]$. The discretised version of (4.10) is given by

$$\dot{\mathbf{u}} = A\mathbf{u} + J\mathbf{u} + \zeta(\tau), \tag{4.11}$$

where $\mathbf{u} = [u_1, u_2, \ldots, u_N]$, $A = \frac{1}{2}\hat{\sigma}^2 D_2 + \left(r - q - \frac{1}{2}\hat{\sigma}^2 - \gamma(\varepsilon)\right) D_1 - (r + \chi(\varepsilon))D_0$. D_2 and D_1 are matrices with entries defined by (A.7) and D_0 is the identity matrix. J and ζ are defined in (4.15) and (4.16), respectively.
For the sake of convenience in the numerical treatment we rewrite the integral part of (4.9) as follows

$$\begin{aligned} J = \int_{\Omega_2} u(x+y,\tau) f(y) dy &= \int_{-\infty}^{+\infty} u(x+y,\tau)\hat{f}(y) dy \\ &= \int_{\mathcal{D}} u(x,\tau)\hat{f}(y-x) dy + \int_{\mathbb{R}\setminus\mathcal{D}} u(y,\tau)\hat{f}(y-x) dy, \end{aligned} \tag{4.12}$$

where

$$\hat{f}(y) = \begin{cases} f(y), & y \in \Omega_2, \\ 0, & y \in \Omega_1. \end{cases} \tag{4.13}$$

We use the Clenshaw-Curtis quadrature rule to compute the first integral over the interval $[y_m, y_M]$ to obtain

$$\begin{aligned} \int_{y_m}^{y_M} u(x,\tau)\hat{f}(y-x) dy &= \frac{1}{2}(y_M - y_m) \int_{-1}^{1} \hat{f}(y-x) u(x,\tau) d\phi, \\ &\approx \frac{1}{2}(y_M - y_m) \sum_{k=0}^{N} \lambda_k \hat{f}(x_k - x_j) u(x_k,\tau) \\ &= J\mathbf{u}(\tau) \end{aligned} \tag{4.14}$$

where $\mathbf{u} = [u_0, u_1, \ldots, u_N]^T$ and J is a $(N+1) \times (N+1)$ matrix with entries

$$(J_{jk})_{0 \leqslant j,k \leqslant N} = \frac{1}{2}(y_M - y_m) \left(\lambda_k \hat{f}(x_k - x_j)\right)_{0 \leqslant j,k \leqslant N}. \tag{4.15}$$

Let $g_L(x,\tau)$ and $g_R(x,\tau)$ be the left and right boundary conditions of the PIDE (4.9). Therefore, the second integral over $\mathbb{R} \setminus [y_m, y_M]$ is approximated using the shifted Laguerre–Gauss quadrature [16] under consideration of the change of variables $\eta = -y + y_m$ for $y < y_m$ and $\eta = y + y_M$ for $y > y_M$. This leads to

$$\begin{aligned} \zeta(x,\tau) &= \int_{-\infty}^{y_m} g_L(x,\tau)\hat{f}(y-x) dy + \int_{y_M}^{\infty} g_R(x,\tau)\hat{f}(y-x) dy, \\ &= -\int_{-y_m}^{\infty} g_L(x,\tau)\hat{f}(y-x) dy + \int_{y_M}^{\infty} g_R(x,\tau)\hat{f}(y-x) dy, \\ &= -\int_{-y_m}^{\infty} g_L(x,\tau)\hat{f}(-y-x) dy + \int_{y_M}^{\infty} g_R(x,\tau)\hat{f}(y-x) dy, \\ &= \int_{0}^{\infty} g_L(x,\tau)\hat{f}(\eta - y_m - x) d\eta + \int_{0}^{\infty} g_R(x,\tau)\hat{f}(\eta + y_M - x) d\eta, \\ &\approx g_L(x,\tau) \sum_{k=0}^{N} \bar{\lambda}_k e^{\eta_k} \hat{f}(\eta_k - y_m - x) + g_R(x,\tau) \sum_{k=0}^{N} \bar{\lambda}_k e^{\eta_k} \hat{f}(\eta_k + y_M - x). \end{aligned} \tag{4.16}$$

4.2 Discretisation of the PIDE on multi sub-domains

On each sub-domain $\mathcal{D}_\nu$, the PIDE can be written as

$$u_\tau^{(\nu)} = \mathcal{A}^{(\nu)}u + \mathcal{B}^{(\nu)}u + \zeta^{(\nu)}(\tau), \quad \nu = 1, 2, \ldots, M, \tag{4.17}$$

where

$$\mathcal{A}^{(\nu)}u = \frac{1}{2}\hat{\sigma}^2 u_{xx}^{(\nu)} + \left(r - q - \frac{1}{2}\hat{\sigma}^2 - \gamma(\varepsilon)\right) u_x^{(\nu)} - (r + \chi(\varepsilon))u^{(\nu)}, \tag{4.18}$$

$$\mathcal{B}^{(\nu)}u = \int_{\mathcal{D}_\nu} u^{(\nu)}(x,\tau)\hat{f}(y-x)dy, \tag{4.19}$$

and

$$\zeta^{(\nu)}(\tau) = \int_{\mathbb{R}\setminus\mathcal{D}} u^{(\nu)}(y,\tau)\hat{f}(y-x)dy. \tag{4.20}$$

Next, we discretise the PIDE (4.9) in the numerical domain $\mathcal{D} = [x_{\min}, x_{\max}]$ by the means of the spectral domain decomposition method described in Section 3. To this end, we divide the domain D into M sub-domains such that

$$\mathcal{D} = \bigcup_{\mu=1}^{M} \mathcal{D}_\mu. \tag{4.21}$$

The discretised version of (4.17) is given by

$$\dot{\mathbf{u}}^{(\nu)} = A^{(\nu)}\mathbf{u}^{(\nu)} + J^{(\nu)}\mathbf{u}^{(\nu)} + \zeta^{(\nu)}, \quad \nu = 1, 2, \ldots, M, \tag{4.22}$$

where

$$\mathbf{u}^{(\nu)} = [u_1^{(\nu)}, u_2^{(\nu)}, \ldots, u_{N_\nu}^{(\nu)}],$$

$$A^{(\nu)}\mathbf{u}^{(\nu)} = \frac{1}{2}\hat{\sigma}^2\mathbf{u}^{(\nu)}D_2^{(\nu)} + \left(r - q - \frac{1}{2}\hat{\sigma}^2 - \gamma(\varepsilon)\right) D_1^{(\nu)}\mathbf{u}^{(\nu)} - (r + \chi(\varepsilon))D_0^{(\nu)}\mathbf{u}^{(\nu)}, \tag{4.23}$$

$$J^{(\nu)}\mathbf{u}^{(\nu)} = \left[(J_{ij})_{1\le i,j\le N_\nu}\right]\mathbf{u}^{(\nu)}, \quad J_{ij}^{(\nu)} = \lambda_j^{(\nu)}\hat{f}^{(\nu)}(x_i - x_j), \tag{4.24}$$

and $I^{(\nu)}u = \zeta(\tau)$ which incorporates the boundary conditions. Letting $L^\nu = A^\nu + B^\nu + I$, Equation (4.22) becomes

$$\dot{\mathbf{u}}^{(\nu)} = L^{(\nu)}\mathbf{u}^{(\nu)} + \zeta^{(\nu)}(\tau). \tag{4.25}$$

The solution on the whole domain $\mathcal{D}$ is given by

$$\dot{\mathbf{u}} = L\mathbf{u} + \zeta(\tau), \tag{4.26}$$

where

$$L = \begin{bmatrix} L^{(1)} & & \\ & \ddots & \\ & & L^{(M)} \end{bmatrix}, \quad \mathbf{u} = \begin{bmatrix} \mathbf{u}^{(1)} \\ \vdots \\ \mathbf{u}^{(M)} \end{bmatrix}, \quad \mathbf{u}^{(\nu)} = \begin{bmatrix} \mathbf{u}_1^{(\nu)} \\ \vdots \\ \mathbf{u}_{N_\nu}^{(\nu)} \end{bmatrix}, \quad \nu = 1, 2, \ldots M. \tag{4.27}$$

Note that when two sub-domains $\mathcal{D}_\nu$ and $\mathcal{D}_{\nu+1}$, touch each other, we apply the continuation conditions of the form

$$\begin{cases} u^{(\nu)}(x)\big|_{x=x_{N_\nu}^{(\nu)}} &= u^{(\nu+1)}(x)\big|_{x=x_1^{(\nu+1)}} \\ \frac{\partial u^{(\nu)}}{\partial x}(x)\Big|_{x=x_{N_\nu}^{(\nu)}} &= \frac{\partial u^{(\nu+1)}}{\partial x}(x)\Big|_{x=x_1^{(\nu+1)}} \end{cases}. \tag{4.28}$$

These last equations are reduced to ODEs when the boundary conditions of a call or put option are imposed in each sub-domains. The obtain ODEs are solved by using Exponential time differencing (ETD) schemes.

4.3 Exponential time differencing schemes

We consider to solve the system of ODEs (4.26)

$$u' = Lu + b(t), \quad u_0 = u(0), \tag{4.29}$$

where L is either a block dense diagonal matrix or a dense matrix depending on the number of domain in consideration, using exponential time differencing methods.
Exponential time differencing (ETD) schemes are known as an alternative to implicit methods for solving stiff systems of ODEs [35, 22, 36]. These methods rely on a fast and stable computation of φ-functions

$$\varphi_0(z) = e^z, \quad \varphi_j(z) = \frac{1}{(j-1)!}\int_0^1 e^{(1-\theta)z}\theta^{j-1}d\theta, \quad j \geq 0, \tag{4.30}$$

i.e., functions of the form $(e^z - 1)/z$. The computation of these functions depends significantly on the structure and the range of eigenvalues of the linear operator and the dimensionality of the semi-discretised PDE. Unfortunately, for spectral methods the linear parts have eigenvalues approaching zero, which leads to complications in the computation of the coefficients. Saad [35], and Hochbruck and Lubich [20] introduced Krylov methods to compute φ-functions. Kassam and Trefethen [22] used Cauchy integral representation on a circle for a stable computation of φ-functions. Other evaluations of exponential and related φ-matrix functions follow the idea of Schmelzer and Trefethen [36]. This method is based on computing optimal rational approximations to the matrix functions on the negative real axis using the Carathéodory-Fejér procedure [42],

The system of ODE (4.29) can be integrated explicitly on the interval [0 T] to give

$$Y(T) \quad = \quad e^{LT}Y(0) + e^{LT}\int_0^T e^{-Lt}b(t)dt. \tag{4.31}$$

The following lemma provides the background for the time stepping procedure for the evaluation of (4.31).

Lemma 4.1. *([30]) The solution of the non-autonomous linear initial value problem*

$$u' = Lu + \sum_{j=0}^{p-1}\frac{\tau^j}{j!}b_{j+1}, \quad u_{\tau_0} = u_0, \tag{4.32}$$

has the solution

$$u(\tau_0 + h) = \varphi(hL)u_0 + \sum_{j=0}^{p-1}\sum_{\ell=0}^{j}\frac{\tau_0^{j-\ell}}{(j-\ell)!}h^{\ell+1}\varphi_{\ell+1}(hL)b_{j+1}. \tag{4.33}$$

The proof of the above lemma can be found in Nielsen and Wright [30]. The computation of the matrix functions φ is obtained by means of the Krylov projection algorithm [30].

5 Numerical results

In this section, we numerically solve the PIDE discretised in Section 4. Two options are used to compare the accuracy of the CGMY, Meixner and GH models on the financial PIDE. We refer as **Example 1**, the case of European call options and as **Example 2**, the case of butterfly call options.

Example 1. We consider a European call option with $K = 50, T = 0.5, r = 0.05, q = 0, \sigma =$

$0.2, \varepsilon = 0.1, x_{\min} = -3$ and $x_{\max} = 1$. The parameters K, T, r, q, σ respectively represent the strike price, the time of maturation, the interest rate, the continuous dividend and the volatility of the underlying asset price. The parameters for Lévy models used in this example and arbitrary chosen for computation purpose and are given in Table 2. Next, we discretise the PIDE (4.9) in the

Model	Parameters
GBM (Black-Scholes)	$K = 50,\ r = 0.05,\ \ \sigma = 0.2,\ \ q = 0$ and $T = 0.5$.
CGMY	$C_- = 0.3,\ C_+ = 0.1,\ \ G = 15,\ M = 25$ and $Y = 20$.
Meixner	$A = 15,\ a = -1.5$ and $b = 50$.
GH	$\alpha = 4,\ \beta = -3.2,\ \delta = 1.4775$ and $\lambda = -3$

Table 2: The parameters for Lévy models used in both examples.

numerical domain $\mathcal{D} = [x_{\min}, x_{\max}]$ by the means of the spectral domain decomposition method described in Section 3 such that

$$\mathcal{D} = \mathcal{D}_1 \cup \mathcal{D}_2 \cup \mathcal{D}_3 \cup \mathcal{D}_4, \tag{5.1}$$

where $\mathcal{D}_1 = [x_{\min}, -\varepsilon]$, $\mathcal{D}_2 = [-\varepsilon, 0]$, $\mathcal{D}_3 = [0, \varepsilon]$ and $\mathcal{D}_4 = [\varepsilon, x_{\max}]$. The domain $\mathcal{D}$ is divided into four sub-domains. Figure 1 (a) represents the matrix structure of L in Equation (4.26) using finite difference and a naive spectral methods for spatial discretisation of the PIDE (4.9). Note that the matrix in Figure 1 (a) in both finite difference and a naive spectral method discretisation. In the case of FD methods, the matrix L is full due to the discretisation of the nonlocal part (4.19). Figure 3 (b) and (c) represent the structure of the matrix L in Equation 4.26, obtained by means of spectral domain decomposition methods where the continuity conditions (4.28) were applied. These block diagonal matrices are preferred to full matrices in a sense that they reduce the number of unknowns and the computational time in solving the linear system (4.29). It is important to note

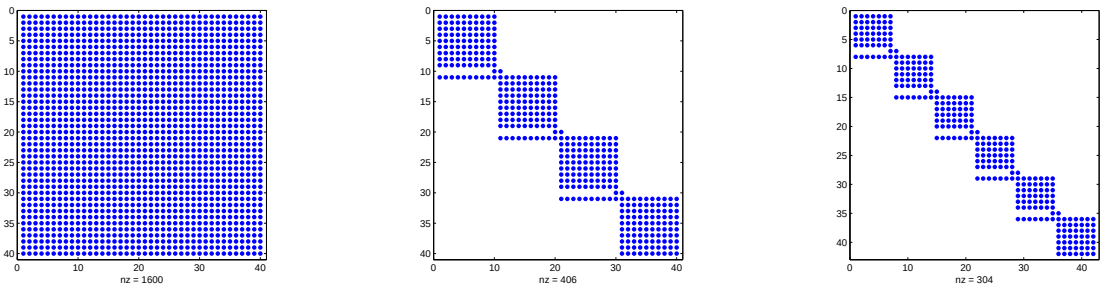

(a) 1 domain (b) 4 sub-domains (c) 6 sub-domains

Figure 1: Spectral domain decomposition method matrix structures

that Figure 1(b) depicts the matrix representation in the case of European call options with four sub-domains, while Figure 1(c) illustrates the case of butterfly spread options with six sub-domains. Figure (2) represents numerical solutions of European call options and their Greeks ($\Delta = \frac{\partial V}{\partial S}$ and

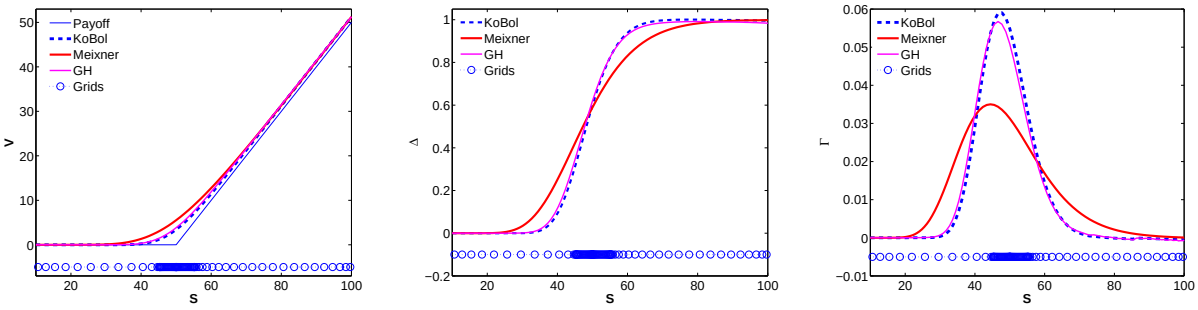

(a) European call (b) Delta (c) Gamma

Figure 2: Numerical valuation of European call options for the KoBoL, Meixner and GH model with their Greeks for the parameters in Table 2.

$\Gamma = \frac{\partial^2 V}{\partial S^2}$) under KoBoL, Meixner and GH Lévy models. The Greeks measure the sensitivity of the option value with respect to the variations in the asset price and the parameters associated with the model [38]. In practice, accurate approximations to Greeks are needed for hedging purposes.

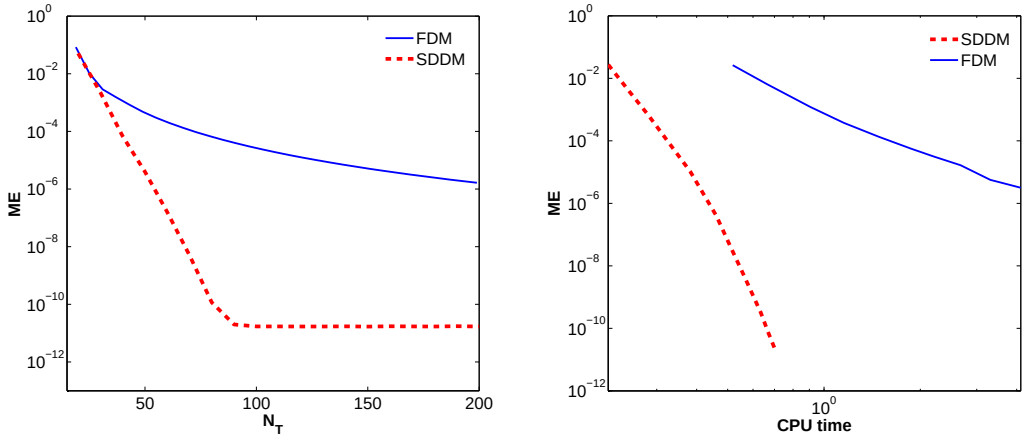

(a) European call option (c) Bull spread call option

Figure 3: Convergence of the SDDM and FDM for European vanilla call options for the parameters in Table 2.

In order to show the superiority of the SDDM over the FDM, we perform some numerical experiments on the case where Equation (2.2) is a geometric Brownian motion leading to a standard Black-Scholes equation. To show the efficiency of the present method we report the the maximal norm error $\mathbf{ME} = \max |U_{Analytical} - U_{Numerical}|$ between analytical solutions (available for the Black-Scholes model) and numerical solutions. In Figure 3, we investigate the tradeoff between computational time (CPU time) and the accuracy as the number of grid points (N_T) increases for European call options. Clearly the SDDM is faster and more accurate than the FDM and achieves spectral convergence as expected.

For the general PIDE (2.5), we report the accuracy of our numerical scheme by means of absolute error $\mathbf{AE} = |U_{Benchmark} - U_{Numerical}|$ where $U_{Benchmark}$ and $U_{Numerical}$ represents the benchmark solution computed with $N = 150$ (the number of grid points in each sub-domain) and the numerical solution, respectively. Table 3 shows the benchmark solution values at $S = \{40, 50, 60\}$ for different Lévy models. We vary the number of grid points N and compute the absolute errors (**AE**) for each

Lévy model. Table 4 represents all the computed **AE** values for each Lévy model with different values of N and S. In all the cases, the number of grid points is chosen to be $N = 100$.

We observe a very rapid decrease of the **AE** as the number of grid points N increases. Note that the approximations of order 10^{-4}, 10^{-5}, 10^{-7} and 10^{-10} in Table 4 are in general difficult to attain with standard finite difference, finite element and finite volume methods.

Model	S		
	40	50	60
KoBoL	0.2210443864	3.3785900783	11.3681462140
Meixner	1.3420365535	5.4934725848	12.7780678851
GH processes	0.3237597911	3.8485639686	11.9164490861

Table 3: The benchmark European call option values under Lévy processes with different values of S and $N = 150$ for the parameters in Table 2.

		$SDDM$				FDM			
	S	40	50	60		40	50	60	
	N	**AE**	**AE**	**AE**	CPU	**AE**	**AE**	**AE**	CPU
KoBoL	10	$1.15e^{-4}$	$1.28e^{-4}$	$1.35e^{-4}$	0.30	$1.14e^{-2}$	$5.72e^{-2}$	$9.55e^{-3}$	0.61
	15	$1.23e^{-5}$	$1.73e^{-5}$	$1.45e^{-5}$	0.34	$2.03e^{-3}$	$1.55e^{-2}$	$1.75e^{-3}$	0.72
	20	$2.75e^{-7}$	$2.13e^{-7}$	$2.34e^{-7}$	0.40	$6.25e^{-4}$	$4.09e^{-3}$	$6.06e^{-4}$	0.87
	25	$3.33e^{-10}$	$3.15e^{-10}$	$3.24e^{-10}$	0.53	$2.75e^{-4}$	$1.91e^{-3}$	$2.37e^{-4}$	1.32
Meixner	10	$2.12e^{-4}$	$2.45e^{-4}$	$2.35e^{-4}$	0.32	$1.46e^{-2}$	$4.35e^{-2}$	$8.51e^{-3}$	0.65
	15	$2.78e^{-5}$	$2.65e^{-5}$	$2.67e^{-5}$	0.35	$2.66e^{-3}$	$1.16e^{-2}$	$2.13e^{-3}$	0.78
	20	$3.40e^{-7}$	$3.23e^{-7}$	$3.14e^{-7}$	0.41	$6.45e^{-4}$	$3.95e^{-3}$	$5.45e^{-4}$	0.86
	25	$4.77e^{-10}$	$4.65e^{-10}$	$4.33e^{-10}$	0.55	$2.35e^{-4}$	$1.02e^{-3}$	$2.14e^{-4}$	1.41
GH processes	10	$3.33e^{-4}$	$3.29e^{-4}$	$3.17e^{-4}$	0.65	$1.45e^{-2}$	$5.33e^{-2}$	$7.13e^{-3}$	1.33
	15	$4.55e^{-5}$	$4.370e^{-5}$	$4.14e^{-5}$	0.82	$2.15e^{-3}$	$1.04e^{-2}$	$5.72e^{-2}$	1.61
	20	$5.14e^{-7}$	$5.21e^{-7}$	$5.14e^{-7}$	1.41	$5.61e^{-4}$	$4.02e^{-3}$	$6.12e^{-4}$	2.94
	25	$7.11e^{-10}$	$7.25e^{-10}$	$7.33e^{-10}$	1.82	$2.36e^{-4}$	$1.21e^{-3}$	$3.01e^{-4}$	3.51

Table 4: Absolute errors (**AE**) of the benchmark and the European call option apply to the KoBoL, Meixner and GH processes models with different values of N and S for the parameters in Table 2.

Example 2. In this subsection, we investigate the performance of our proposed method for valuing European butterfly options under Lévy models at the strike prices $K_1 = 40$, $K_2 = 50$ and $K_3 = 60$ using the parameters presented in Table 2 and in **Example 1**. In this particular case, we need to divide the domain at five different points, namely three different strike prices (K_1, K_2 and K_3), and at two singularities ($-\varepsilon$ and ε) present in the kernel of the integral (4.13)). Figure 4 represents numerical solutions of European butterfly call options and their Greeks ($\Delta = \frac{\partial V}{\partial S}$ and $\Gamma = \frac{\partial^2 V}{\partial S^2}$) under the KoBoL, Meixner and GH Lévy models.

In Figure 5 we investigate the tradeoff between computational time and the accuracy as the number of grid points increases for European vanilla butterfly call options. Clearly the SDDM is faster and more accurate than the FDM and achieves spectral convergence as expected.

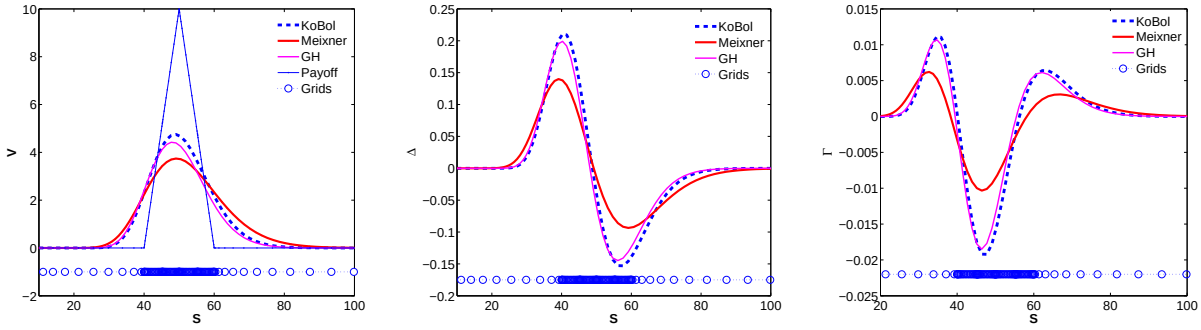

(a) European butterfly call (b) Delta (c) Gamma

Figure 4: Numerical valuation of European butterfly call options for the KoBoL, Meixner and GH model with $N = 16, K_1 = 40, K_2 = 50, K_3 = 60$ for the parameters in Table 2.

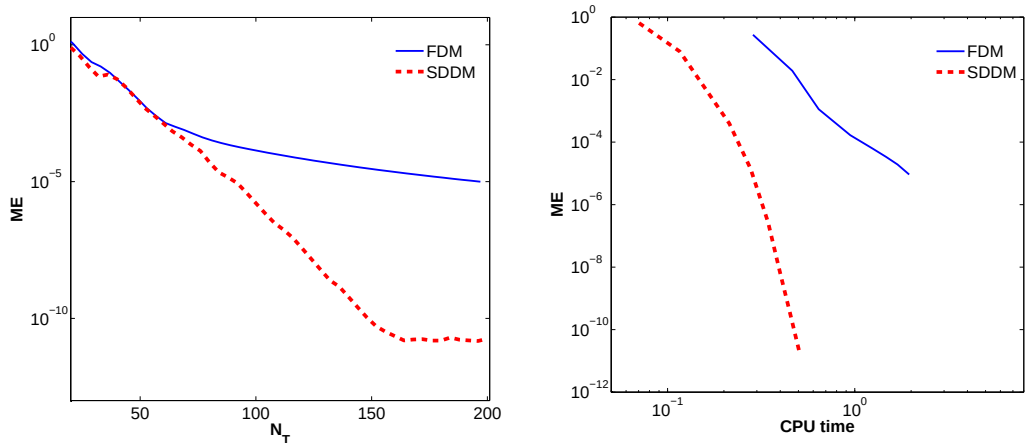

(a) European call option (c) Butterfly call option

Figure 5: Convergence of the SDDM and FDM for European vanilla butterfly call options for the parameters in Table 2.

Model	S		
	40	50	60
KoBoL	2.2845953002	4.6814621409	2.1592689295
Meixner	2.2689295039	3.7101827676	2.3159268929
GH processes	2.3942558746	4.2898172323	1.7989556135

Table 5: The benchmark values of the European butterfly call option values under Lévy processes with different values of S and $N = 100$ for the parameters in Table 2.

Table 5 shows the benchmark prices of butterfly call options. Table 6 depicts the **AE** between benchmark prices and numerical solutions of each model with different values of N and S. We observe a very rapid convergence in the case of European butterfly spread option which has five regions of singularity. Our approach allows a high resolution of grids around the strike prices K_1, K_2 and K_3, and at two singularities $-\varepsilon$ and ε present in the kernel of the integral (4.13). Once

		SDDM				*FDM*			
	S	40	50	60		40	50	60	
	N	**AE**	**AE**	**AE**	CPU	**AE**	**AE**	**AE**	CPU
KoBoL	07	$1.88e^{-4}$	$1.76e^{-4}$	$1.76e^{-4}$	0.20	$1.24e^{-2}$	$5.81e^{-2}$	$8.98e^{-3}$	0.62
	10	$1.45e^{-5}$	$1.81e^{-5}$	$1.71e^{-5}$	0.28	$1.98e^{-3}$	$1.63e^{-2}$	$2.05e^{-3}$	0.73
	13	$2.91e^{-7}$	$2.33e^{-7}$	$2.25e^{-7}$	0.33	$5.99e^{-4}$	$4.29e^{-3}$	$5.66e^{-4}$	0.87
	16	$3.72e^{-10}$	$3.34e^{-10}$	$3.81e^{-10}$	0.44	$2.83e^{-4}$	$2.11e^{-3}$	$2.48e^{-4}$	1.41
Meixner	07	$2.45e^{-4}$	$3.32e^{-4}$	$3.22e^{-4}$	0.24	$1.56e^{-2}$	$4.28e^{-2}$	$8.88e^{-3}$	0.63
	10	$2.72e^{-5}$	$2.75e^{-5}$	$2.46e^{-5}$	0.24	$1.99e^{-3}$	$1.23e^{-2}$	$2.34e^{-3}$	0.75
	13	$3.54e^{-7}$	$3.28e^{-7}$	$3.69e^{-7}$	0.34	$6.25e^{-4}$	$4.05e^{-3}$	$5.32e^{-4}$	0.85
	16	$5.68e^{-10}$	$5.55e^{-10}$	$5.88e^{-10}$	0.42	$2.44e^{-4}$	$1.24e^{-3}$	$2.51e^{-4}$	1.42
GH processes	07	$3.12e^{-4}$	$3.02e^{-4}$	$3.45e^{-4}$	0.51	$1.25e^{-2}$	$5.71e^{-2}$	$6.97e^{-3}$	1.32
	10	$5.51e^{-5}$	$6.1e^{-5}$	$5.92e^{-5}$	0.68	$2.13e^{-3}$	$1.21e^{-2}$	$5.87e^{-2}$	1.63
	13	$7.11e^{-7}$	$7.25e^{-7}$	$7.33e^{-7}$	0.82	$5.11e^{-4}$	$4.14e^{-3}$	$6.22e^{-4}$	2.91
	16	$8.25e^{-10}$	$9.12e^{-10}$	$9.23e^{-10}$	1.32	$2.53e^{-4}$	$1.31e^{-3}$	$3.12e^{-4}$	3.48

Table 6: Absolute errors (**AE**) of the benchmark and the European call option apply to the KoBoL, Meixner and GH processes models with different values of N and S for the parameters in Table 2.

again, we obtain approximations of order 10^{-4}, 10^{-5}, 10^{-7} and 10^{-10} in Table 6.

6 Conclusion

We have presented a spectral domain decomposition method coupled with the exponential time integrator (4.31) for pricing European call and European butterfly call options for a class of infinite activity Lévy models, including the KoBoL, Meixner and GH models. Our method produced fast and very accurate results for **Example 1** and **2** as compared to FDM. Furthermore the computed Greeks were free of spurious oscillations. Currently, we are investigating our approach to solve multi-asset Lévy models.

References

[1] A. Almendral and C. W. Oosterlee, Accurate evaluation of European and American options under the CGMY process, *SIAM Journal on Scientific Computing* **29(1)** (2007) 93-117.

[2] R. Baltensperger, J. P. Berrut, and B. Noël, Exponential convergence of a linear rational interpolant between transformed Chebyshev points, *Mathematics of Computation* **68** (1999) 1109-1120.

[3] J. P. Berrut and H. D. Milltelmann, Rational interpolation through the optimal attachment of poles to the interpolating polynomial, *Numerical Algorithms* **23(4)** (2000) 315-328.

[4] J. P. Berrut and L. N. Trefethen, Barycentric Lagrange Interpolation, *SIAM Review* **46(3)** (2004) 501-517.

[5] F. Black and M. Scholes, Pricing of options and corporate liabilities, *Journal of Political Economy* **81(3)** (1973) 637-654.

[6] M. Briani, C. La Chioma and R. Natalini, Convergence of numerical schemes for viscosiy solutions to integro-differential degenerate parabolic problems arising in financial theory, *Journal of Numerical Mathematics* **98(4)** (2004) 607-646.

[7] P. Carr, H. German, D. B. Madan and M. Yor, The fine structure of asset returns : An empirical investigation, *Journal of Business* **75** (2002) 305-332.

[8] T.F. Coleman, Y. Li and A Verma, Reconstructing the unknown local volatility function, *Journal of Computational Finance* **2** (1999) 77-100.

[9] R. Company, L. Jódar, M. Fakharany, Positive solutions of European option pricing with CGMY process models using double discretization difference schemes, *Abstract and Applied Analysis* (2013) Article ID 517480, 11 pages.

[10] R. Cont and E. Voltchkova, A finite difference scheme for option pricing in jumps diffusion and exponential Lévy models, *SIAM Journal on Numerical Analysis* **43(4)** (2005) 1596-1626.

[11] R. Cont, E. Voltchkova, A finite difference scheme for option pricing in jump diffusion and exponential Lévy models, *SIAM Journal on Numerical Analysis* **43 (4)** (2005) 1596–1626.

[12] Y. d'Halluin, P.A. Forsyth and K.R. Vetzal, Robust numerical methods for contigent claims under jump-diffusion processs, *IMA Journal of Numerical Analysis* **25(1)** (2005) 87-112.

[13] P.J. Davis and P. Rabinowitz, *Methods of numerical integration*, Academic Press Inc., Orlando, FL, 2nd edition, 1984.

[14] B. Dupire, Pricing with a smile, *RISK Magazine* **1** (1994) 18-20.

[15] M. Fakharany, R. Company, L. Jódar, Solving partial integro-option pricing problems for a wide class of infinite activity Lévy processes, *Journal of Computational and applied Mathematics* **296** (2016) 739-752.

[16] R. Frontczak and R. Söchbel, On modified Mellin transforms, Gauss–Laguerre quadrature, and the valuation of American call options, *Journal of Computational and Applied Mathematics* **234** (2010) 1559-1571.

[17] D. Funaro, *Polynomial Approximation of Differential Equations*, Springer, Berlin, 1992.

[18] D. Gottlieb and C. -W. Shu, On the Gibbs phenomenon IV: Recovering exponential accuracy in a subinterval from a Gegenbauer partial sum of a piecewise analytic function, *Journal of Computational and Applied Mathematics* **64** (1995) 1081-1095.

[19] S. Heston, A closed-form solution for options with stochastic volatility with applications to bond and currency options, *Review of Financial Studies* **6** (1993) 327-343.

[20] M. Hochbruck and C. Lubich, On Krylov subspace approximations to the matrix exponential operator, S*IAM Journal of Numerical Analysis* **34** (1997) 1911-1925.

[21] J. Hull and A White, The pricing of options with stochastic volatilities, *Journal of Finance* **42** (1987) 281-300.

[22] A.K. Kassam and L.N. Trefethen, Fourth-order time stepping for stiff PDEs, *SIAM Journal of Scientific Computing* **26** (2005) 1214-1233.

[23] G. Klein and J.P. Berrut, Linear barycentric rational quadrature, *BIT Numerical Mathematics* **52** (2012) 407-424.

[24] P. E. Kloeden, G. J. Neuenkirch and T. Shardlow, The exponential integrator scheme for stochastic partial differential equations: Pathwise error bounds, *Journal of Computational and Applied Mathematics* **235(5)** (2011) 1245-1260.

[25] S.G.Kou, A Jump-Diffusion Model for Option Pricing, *Management Science* **8(48)** (2002) 1086-1101.

[26] J. L. Lagrange, Leçons élémentaires sur les mathématiques, *données à l'Ecole Normal en 1795, in Oeuvres VII, Gauthier-Villars, Paris*, **7** (1877) 183-287.

[27] D.B. Madan and E. Seneta, The variance gamma model for share market returns, *Journal of Business* **63** (1990) 511-524.

[28] C. Markakis, and L. Barack, High-order difference and pseudospectral methods for discontinuous problems, *arXiv: 1406.4865v1 [maths.NA]*, (2014) 1-9.

[29] R.C. Merton, Option pricing when the underlying stocks are discontinuous, *Journal of Financial Economics* **5** (1976) 125-144.

[30] J. Niesen and W. M. Wright, A Krylov subspace method for option pricing, Technical report SSRN 1799124, 2011

[31] H. K. Pang and H. W. Sun, Fast exponential time integration for pricing options in stochastic volatility jump diffusion models, *East Asian Journal on Applied Mathematics* **4(1)** (2014) 52-68.

[32] H. P. Pfeiffer, L. E. Kidder, M. A. Scheel, and S. A. Teukolsky, A multidomain spectral method for solving elliptic equations, *Computer Physics Communications* **152** (2003) 253-273.

[33] E. Pindza, K.C. Patidar and E. Ngounda, Robust Spectral Method for Numerical Valuation of European Options under Merton's Jump-Diffusion Model, *Numerical Methods for Partial Differential Equations* **30(4)** (2014) 1169-1188.

[34] N. Rambeerich, D. Y. Tangaman, M. Bhuruth, Numerical Pricing Of American Option Under Infinite Activity Lévy Processes, *Journal of Futures Markets* **31(9)** (2011) 809-829.

[35] Y. SAAD, Analysis of some Krylov subspace approximations to the matrix exponential operator, *SIAM Journal of Numerical Analysis* **29** (1992) 209-228.

[36] T. Schmelzer and L. N. Trefethen, Evaluating Matrix Functions for Exponential Integrators via Carathéodory-Fejér Approximation and Contour Integrals, *Electronic Transactions on Numerical Analysis* **29** (2007) 1-18.

[37] D. Y. Tangman, A. Gopaul and M. Bhuruth, Exponential time integration and Chebyshev discretisation schemes for fast pricing options, *Applied Numerical Mathematics* **58(9)** (2008) 1309-1319.

[38] D. Tavella and C. Randall, *Pricing Financial Instruments: The Finite Difference Method*, Wiley, New York, 2000.

[39] L.N. Trefethen, *Approximation Theory and Approximation Practice*, SIAM, Philadelphia, PA, 2013.

[40] L.N. Trefethen, Is Gauss quadrature better than Clenshaw–Curtis? *SIAM Review* **50 (1)** (2008) 67-87.

[41] L.N. Trefethen, Spectral Methods in Matlab, SIAM, Philadelphia, PA, 2000.

[42] L.N. Trefethen and H.M. Gutknecht, The Carathéodory-Fejér method for real rational approximation, *SIAM Journal on Numerical Analysis* **20** (1983) 420-436.

[43] I. R. Wang, J. W. Wan, and P. A. Forsyth, Robust numerical valuation of European and American options under the CGMY process, *Journal of Computational Finance* **10(4)** (2007) 31-69.

[44] B.D. Welfert, Generation of pseudospectral differentiation matrices I, *SIAM Journal on Numerical Analysis* **34** (1997) 1640-1657.

[45] W. Schoutens and J.L. Teugels, Lévy processes, polynomials and martingales, *Communications in Statistics. Stochastic Models* **14 (1-2)** (1998) 335-349.

[46] D. Madan and M. Yor, Representing the CGMY and Meixner Lévy processes as time changed Brownian motions, *Journal of Computational Finance* **12 (1)** (2008) 27-47.

[47] W. Schoutens, *Lévy Processes in Finance: Pricing Financial Derivatives*, Wiley, New York, 2003.

Appendices

A Numerical interpolations and applications

In practice, we are often confronted with situations where only limited amount of data is accessible and it is necessary to estimate values between two consecutive given data points. We can construct new points between known data points by interpolation or smoothing techniques. In finance, as only a finite set of securities are traded in financial markets, it is very important to construct a sensible curve or surface from discrete observable quantities using interpolation methods.
In this section, we review concept of interpolation, differentiation matrix and quadrature rule in barycentric spectral method framework in one domain and multi-domains.

A.1 Spectral barycentric interpolation

The review done by [3] on the Lagrange interpolation and the barycentric formula shows the importance of the discretization in space with spectral methods. At first, a polynomial $u_N(x)$ is considered to be found among the vector space of all polynomials of degree N such that $u_N(x_j) = u_j$ with $j = 0, ..., N$. The result can be written in Lagrange form as ([26])

$$u_N(x) = \sum_{j=0}^{N} u_j \phi_j(x), \;\; \phi_j = \prod_{k=0, k\neq j}^{N} \frac{x - x_k}{x_j - x_k}, \tag{A.1}$$

with Lagrange polynomial ϕ_j corresponding to the node x_j having the property

$$\phi_j(x_k) = \begin{cases} 1 & \text{when} \quad j = k \\ 0 & \text{otherwise.} \end{cases} . \tag{A.2}$$

The evaluation of (A.1) requires an $\mathcal{O}(N^2)$ additions and multiplications. In addition the presence of instability in the numerical computation is certain. Therefore, a modifications of (A.1) is required to overcomes those disadvantages. Hence, Berrut and Trefethen [4] proposed a more stable barycentric formula of (A.1) that allows the computation of $u_N(x)$ in $\mathcal{O}(N)$ operations. The new formula is written as

$$u_N(x) = \sum_{j=0}^{N} u_j \phi_j(x), \quad \phi_j = \frac{\frac{\omega_j}{x-x_j}}{\sum_{j=0}^{N} \frac{\omega_j}{x-x_j}}, \quad \omega_j = \frac{1}{\prod_{k\neq j}(x_j - x_k)}, \tag{A.3}$$

where $w_0, w_1, \ldots, w_N$ are called barycentric weights.
It is a well known that an adequate choice of nodes contributes in a decisive manner to improve the accuracy of the approximation and reduce the computational effort. In this paper, a valuable selection is the well-known Chebyshev-Gauss-Lobatto (CGL) nodes $x_k = cos(\frac{k\pi}{N})$, $k = 0, 1, 2, ..., N$, [17, 41], which are not uniformly distributed but clustered near the endpoints. The corresponding set of barycentric weights is $w_0 = c/2$, $w_k = (-1)^k c, k = 1, \ldots, N-1$, and $w_N = (-1)^N c/2$ for some non-zero constant c [2]. Note that for every set of points $\{x_k\}$, there is a unique set of barycentric weights $\{w_k\}$. More details are given in [4] to obtain (A.3).

A.2 Differentiation matrix

An important task in pseudo-spectral methods is to compute the derivatives $u^{(p)}(x)$ in terms of the values of $u(x)$ at the collocation points x_k. A common, practical and efficient way is the use of differentiation matrix which allows to perform the numerical differentiation in a straightforward way in terms of matrix–vector products. For $u(x)$ sufficiently smoothness and p positive integer number, one can approximate the p^{th} derivative of $u(x)$ by

$$u_N^{(p)}(x) = D^{(p)} u, \tag{A.4}$$

where the entries of the p-order differentiation matrix $D^{(p)}$ are given by

$$d_{jk}^{(p)} = \phi^{(p)}(x_j), \quad j, k = 0, \ldots, N. \tag{A.5}$$

Welfert [44] proposed the following hybrid formula to compute the entries of the p-th order differentiation matrix,

$$d_{jk}^{(p)} = \begin{cases} \dfrac{p}{(x_j - x_k)} \left(\dfrac{\omega_k}{\omega_j} d_{jj}^{(p-1)} - d_{jk}^{(p-1)} \right) & \text{if } j \neq k, \\ -\displaystyle\sum_{i=0, i\neq k}^{N} d_{ji}^{(p)}, & \text{if } j = k. \end{cases} \tag{A.6}$$

In the above, the entries of the first and the second differentiation matrices $D^{(1)}$ and $D^{(2)}$ are given as ([44]):

$$d_{jk}^{(1)} = \begin{cases} \dfrac{\omega_k}{\omega_j(x_j - x_k)} & \text{if } j \neq k, \\ -\displaystyle\sum_{i=0, i\neq j}^{N} d_{ji}^{(1)} & \text{if } j = k, \end{cases}, \qquad d_{jk}^{(2)} = \begin{cases} 2d_{jk}^{(1)}\left(d_{jj}^{(1)} - \dfrac{1}{x_j - x_k}\right) & \text{if } j \neq k, \\ -\displaystyle\sum_{i=0, i\neq j}^{N} d_{ji}^{(2)}, & \text{if } j = k, \end{cases} \tag{A.7}$$

where $j, k = 0, 1, \ldots, N$. These differentiation matrices are more stable, with respect to rounding errors, than direct evaluation [44]. In view of the above setting, the rational collocation interpolation (A.3) enjoys exponential convergence property as stated in the following theorem.

Theorem A.1. *([39]). Let $u(x)$ be analytic in [-1, 1]. Then, there exists a constant $\rho > 1$ such that for any integer $p \geq 0$ such that*

$$\max_{x\in[-1,1]} \left| u^{(p)}(x) - u_N^{(p)}(x) \right| = \mathcal{O}(\rho^{-N}). \tag{A.8}$$

The constant ρ refers to the Bernstein ellipse E_ρ in which u is analytically continuable. For large regions in the complex plane in which u is analytical, the interpolation polynomials u_N has a faster convergence to u as N grows (and the same holds for the respective derivatives).

A.3 Spectral barycentric quadrature

Let u be a real function and $N+1$ the number of sampled points. The approximation or linear quadrature rule $I \approx \sum_{j=0}^{N} \lambda_j u_j$ of the integral $I = \int_a^b u(x)dx$ can be achieved by two different ways:

- non-uniform grids, e.g. Gauss or Clenshaw–Curtis quadrature;
- uniform or equispaced points, e.g. the Newton–Cotes, trapezoidal rule, Simpson or Boole.

In this article, we consider the Clenshaw–Curtis quadrature. We now show how the replacement of polynomial by linear rational interpolation leads to quadrature formulas which allow arbitrarily large numbers of equispaced nodes. Clearly, every linear interpolation formula trivially yields a linear quadrature rule. For a barycentric rational interpolant, we have:

$$\int_a^b u(x)dx = \int_a^b p_N(x)dx = \int_a^b \frac{\sum_{j=0}^{N} \frac{\omega_j}{x-x_j} u_j}{\sum_{j=0}^{N} \frac{\omega_j}{x-x_j}} dx = \sum_{j=0}^{N} \lambda_j u_j, \tag{A.9}$$

where

$$\lambda_j = \int_a^b \frac{\frac{w_j}{x-x_j}}{\sum_{j=0}^{N} \frac{w_j}{x-x_j}} dx \tag{A.10}$$

is the integral of the j^{th} Lagrange fundamental rational function. There are two different ways to compute (A.10):

- On one hand, one can use the direct rational quadrature. The technique consists of applying existing quadrature rules such as Gauss–Legendre or Clenshaw–Curtis [13, 40], which are known to perfectly approximate the integrals in (A.10).

- On the other hand, we can apply the indirect rational quadrature. This may produce the integral $I = \int_a^b u(x)dx$ through the solution of an ordinary differential equation, see e.g. [23].

The Clenshaw-Curtis quadrature formula has the following convergence property.

Theorem A.2 ([13, 40])**.** *Let f an analytic function in $[-1, 1]$ and analytically continuable with $|f(z)| < M$ in the closed ellipse E_ρ. The error in $I_N(f)$, the Clenshaw-Curtis quadrature of degree N to $I(f)$, will decay geometrically with the bound*

$$|I - I_N| \leq \frac{64M}{15(\rho^2 - 1)(\rho^{N-1} - \rho^{-(N-1)})}, \quad N \geq 3 \text{ odd.} \tag{A.11}$$

In other words,

$$|I - I_N| = \mathcal{O}(\rho^{-N}). \tag{A.12}$$

Proof. See [13].
The main advantage with the Clenshaw-Curtis quadrature rule is that its weights and nodes can be computed efficiently via a fast Fourier transform (FFT) in only ($\mathcal{O}(N \ln N)$) operations.